Landslide Susceptibility Mapping Using GIS-Based Frequency Ratio Approach in Part of Kullu District, Himachal Pradesh, India

Baboo Chooreshwarsingh Sujeewon and Raju Sarkar

1 Introduction

Landslide, a type of mass wasting, is defined as the downslope movement of slope forming materials by gravitational force.

Landslide occurrences in Himachal Pradesh have increased due to extreme climatic conditions coupled with rise in man-made activities which can be attributed to the high surge in tourism, hydropower generation, industrialization and road construction in the area ([3]). These catastrophic events entail severe socio-economic impact [9] through disruption of local businesses in terms of road blockage, destruction to infrastructure and loss of human life. Landslide susceptibility analysis is one important pre-hazard management tools used to delineate an area according to its degree of susceptibility to landslide incidence [6].

The most common susceptibility mapping approaches adopted by researchers are broadly classified as heuristic, statistic, deterministic and hybrid.

Heuristic approach (also known as knowledge-driven or qualitative) can be direct or indirect in nature, relying on knowledge of experts for geomorphological mapping or weight assignment of landslide causative factors thereby introducing a degree of subjectivity, whereas statistical (also known as data-driven or quantitative) approach can be grouped as bi-variate [4] and multi-variate methods, both based on the assumption that the combination of past and present landslides contributing factors aid in predicting future slides under the same condition [2].

Bi-variate approaches such as frequency ratio, information value, weight of evidence, etc., rely on the association of each parameter class to past landslide

B. C. Sujeewon (✉) · R. Sarkar
Delhi Technological University, New Delhi, India
e-mail: sujeewon_mt2k19@dtu.ac.in

R. Sarkar
e-mail: rajusarkar@dce.ac.in

B. R. Adhikari and S. Kolathayar (eds.), *Geohazard Mitigation*, Lecture Notes in Civil Engineering 192, https://doi.org/10.1007/978-981-16-6140-2_16

occurrence instead of relative weight determination between factors [11] compared to multi-variate methods.

This paper is an attempt to delineate regions in the study area based on their proneness to landslides through a frequency ratio (FR) based landslide susceptibility mapping using geographical information system (GIS) environment and to understand the spatial link between the nine considered landslide-inducing factors with the updated landslide inventory. This inter-relationship can reveal patterns unique to the geographical area for better evaluation of landslide occurrences.

2 Study Area

The district of Kullu, one of the twelve districts of the state of Himachal Pradesh is bounded between 31° 20′ to 32° 26′ East and 76° 56′ to 77° 52′ North and located in the north-western Himalayan region of India as shown in Fig. 1. Bordering the district concerned are the districts of Lahaul and Spiti (North and North-east), Kangra (North-west), Kinnaur (South-east), Shimla (South and South-east) and Mandi (South-west to West). It includes four tehsils (Manali, Kullu, Banjar and Nirmand) and two sub-tehsils (Sainj and Anni) with an average annual rainfall of 1405.7 mm.

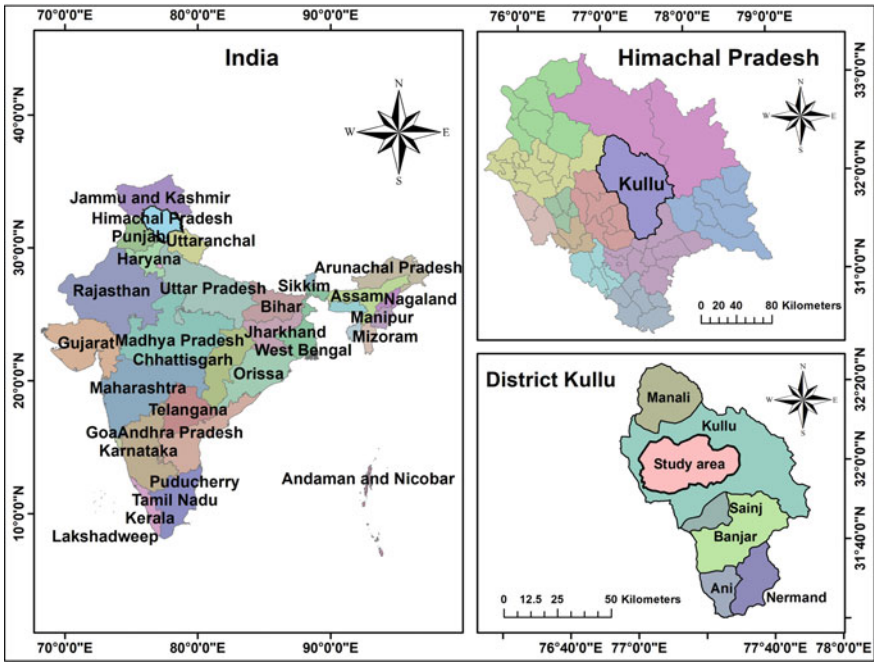

Fig. 1 Locator map of study area

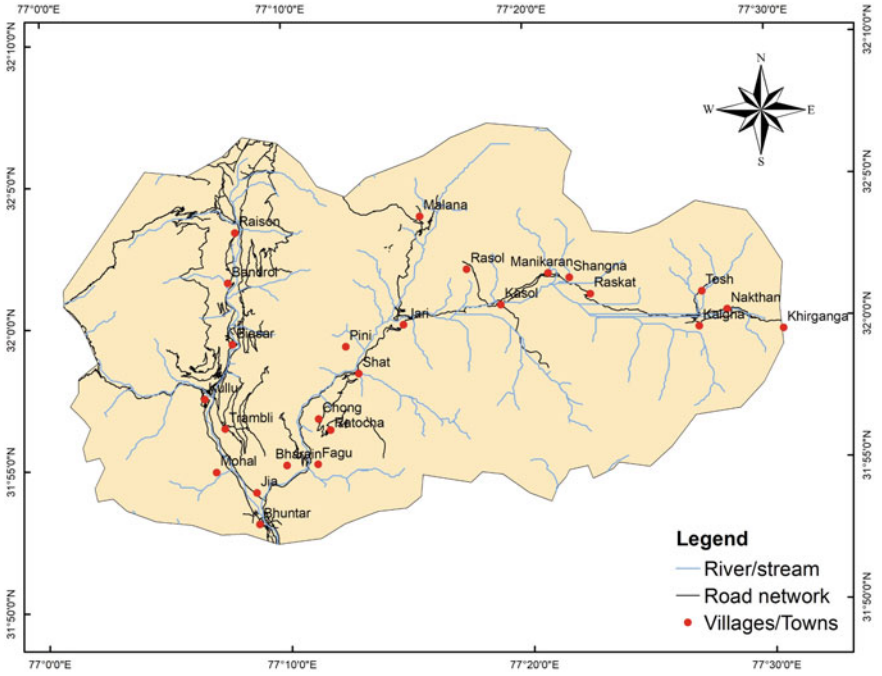

Fig. 2 Study area

The research area (part of the Kullu tehsil) as depicted in Fig. 2, covers an area of around 1000 km^2 with elevation ranging from 1050 to 4900 m. It is accessible by flight through the nearest airport at Bhuntar or by land through the major road networks in the area which are the national highway NH-3 and the major district roads of Kullu-Nagar-Manali and Jia-Manikaran.

Kullu and Kasol-Manikaran valleys run along the Beas and Parvati River attracting a considerable number of tourists with important and famous places like Kullu, Bhuntar, Malana, Kasol, Tosh, Khirganga.

3 Methodology

The adopted methodology in this study constitutes: (a) preparation of a compiled landslide incidence map; (b) selection of landslide-inducing factors and thematic maps generation; (c) frequency ratio calculation for each factor class; (d) landslide susceptibility index evaluation for each factor; (e) creation and classification of the final landslide susceptibility map; (f) model validation through the Area Under Curve (AUC) and Landslide Density Index (LDI) methods.

4 Data Preparation

Factors such as slope, aspect, curvature and drainage network were extracted using different tools from CartoSAT-1 DEM (spatial resolution of about 30 m) obtained from the web-based platform of Bhuvan, Indian Space Research Organization (ISRO), National Remote Sensing Centre (NRSC), Hyderabad.

Digital shape files for faults, lineaments, past landslides and lithology were obtained from Bhukosh, Geological Survey of India (GSI) and shape file for road network in the area was retrieved from Open Street Map website.

Landsat-8 images were obtained from the Earth Explorer, U.S. Geological Survey (USGS) for land use and land cover classification.

4.1 Landslide Inventory

Past landslide inventory for the study area was obtained from past literatures and Bhukosh web-platform of the Geological Survey of India (GSI) as shown in Fig. 3a. Clustering of most historical data near the Kullu-Bhuntar led to the creation of a new landslide inventory near the Parvati valley area through visual interpretation of high-resolution satellite imagery from Google Earth for the year 2002–2019. Change in vegetation and the presence of debris material were amongst the main criteria used for landslide mapping using Google Earth historical images [5].

Landslide scars can be rapidly lost or obscured with time due to excess vegetation, remediation works, etc. The use of scarp identification and contour connection method (SICCM) toolbox was made for semi-automatic scarp delineation of some obscured landslide features [2].

The compiled landslide incidence shape file consisting of 211 total mapped landslide polygons was resampled in cell resolution of 30×30 m for further processing. Random splitting of samples into training (70% $\approx$ 147 no.) and validating (30% $\approx$ 64 no.) datasets were done using a geostatistical analyst tool as shown in Fig. 3(b). Ground truthing for the newly mapped landslide locations was not carried out due to remoteness and travel limitation.

4.2 Thematic Maps Preparation

Nine causative factors were selected based on past literatures in the area and data availability. Nine thematic layers were then prepared in a GIS environment as in Figs. 4 and 5 for correlation analysis with landslide occurrence using the frequency ratio-based statistical method.

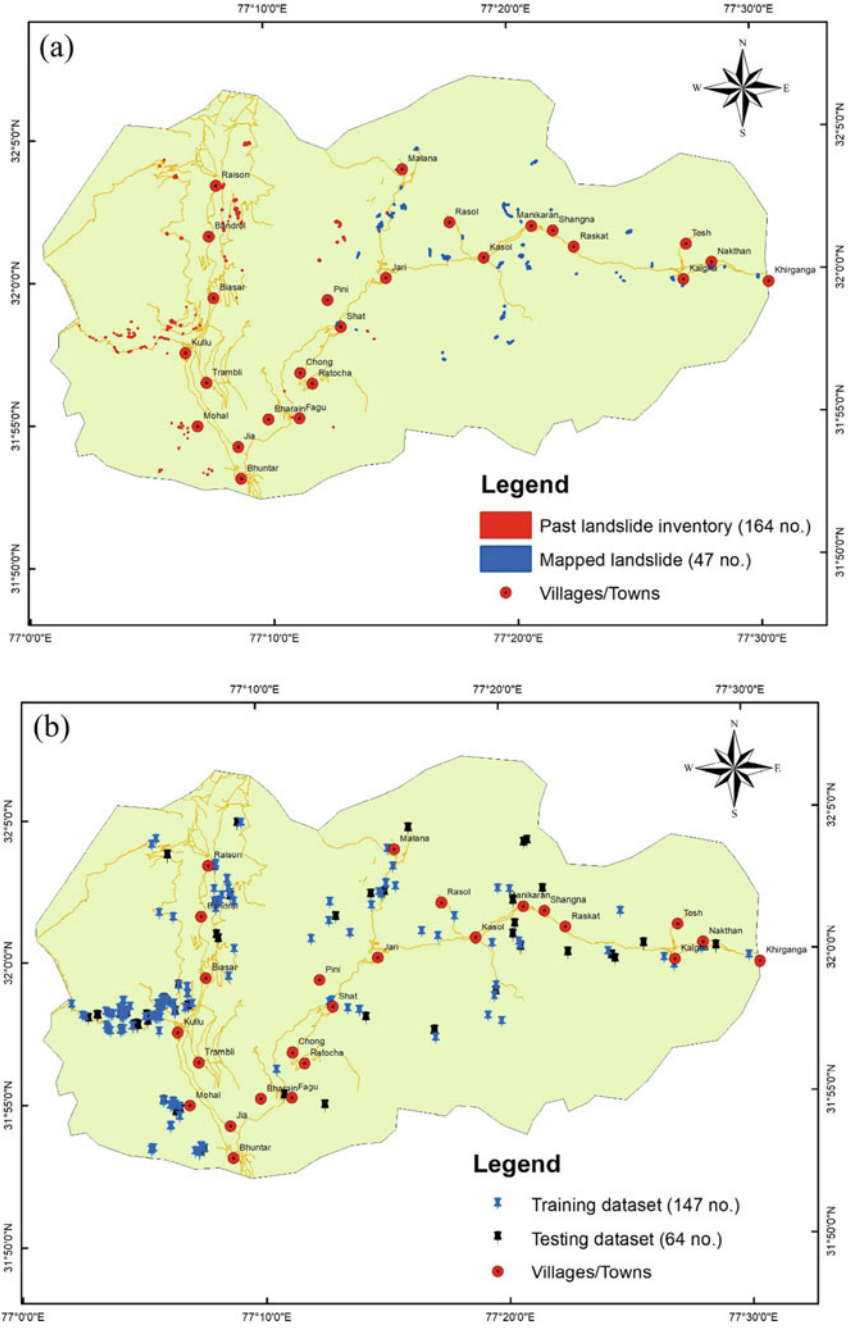

Fig. 3 Landslide inventory: **a** Past and updated inventory. **b** Training and testing datasets

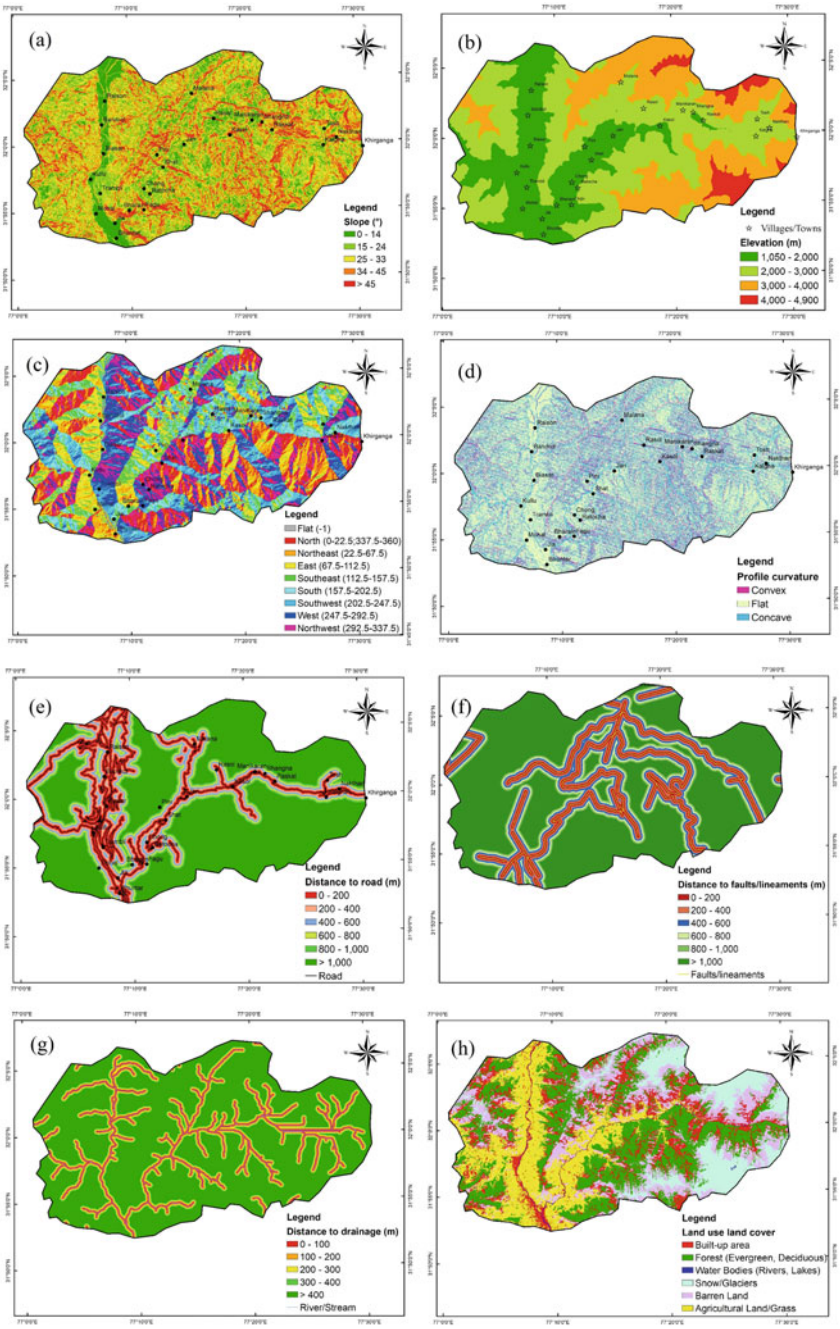

Fig. 4 **a** Slope map. **b** Elevation map. **c** Aspect map. **d** Profile curvature map. **e** Distance to road map. **f** Distance to faults/lineaments map. **g** Distance to drainage map. **h** Land use land cover map

Slope.

Slope map depicts the angle of slope of a particular area and is directly related to slope instability [2].

The slope map is derived from the CartoSAT-1 Digital Elevation Model (DEM) using surface (spatial analyst) tools in GIS platform. The resulting map is reclassified into five distinct classes namely 0°–14°, 15°–24°, 25°–33°, 34°–45°, >45° as in Fig. 4a.

Aspect.

The aspect map (Fig. 4c) indicates the facing direction of slopes. The direction faced by the slope is measured and classified from the DEM clockwise starting North at 0° back to North at 360° using the aspect tool in GIS platform. Flat areas (no slope and aspect) are denoted by grey cells with value –1.

Different slope orientations are exposed to different amount of direct sunlight and wind exposure along with other factors affecting vegetation type, vegetation density, soil moisture index, etc.

Curvature.

The profile curvature map derived from the DEM using curvature (spatial analyst) tool, indicates the degree of convexity/concavity of surfaces and also influences the acceleration/deceleration rate of surficial flows.

The resulting map has three classes with negative values (<–0.05) for convex surfaces, positive values (>0.05) for concave surfaces and near zero values (–0.05 to 0.05) for linear surfaces as in Fig. 4d.

Distance to drainage.

The distance to drainage map was created using the hydrology tools for stream order generation from the DEM and then the Euclidean distance tool was used for buffer at intervals of 100 m from stream network. The resulting map was divided into five distinct classes namely 0–100 m, 100–200 m, 200–300 m, 300–400 m and >400 m as in Fig. 4g.

Changes in the surface water levels along rivers affects slope saturation along the banks, pore water pressure and internal strength of slope forming material due to infiltration. High-rainfall intensity is followed by high-river discharge capacity causing bank erosion.

Elevation.

Elevation indirectly affects landslide occurrences since it influences other important factors such as vegetation type, rainfall intensity, temperature, wind exposure, etc.

Triangulated irregular networks (TIN) were generated from contour lines of the area before being converted and classified into the final elevation raster with four groups; 1050–2000 m, 2000–3000 m, 3000–4000 m and 4000–4900 m as in Fig. 4b. Human intervention is scarce at higher elevations (>4000 m) with lesser extent of land available and the presence of snow/glaciers all year round.

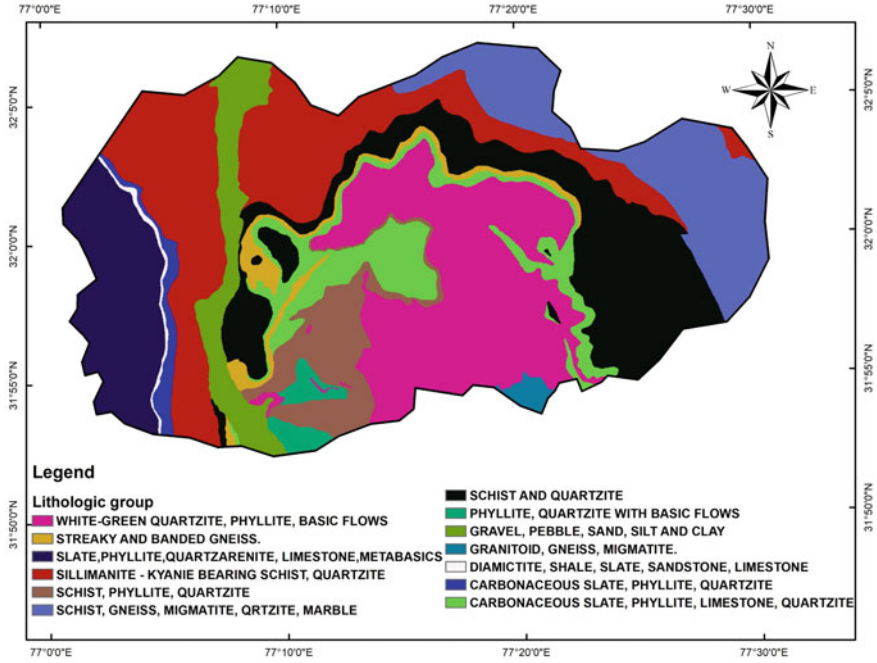

Fig. 5 Lithology map

Lithology.

The structure, strength, composition and plasticity potential for each unit are different [7], hence their individual influence on landslide incidence need to be evaluated.

The lithology digital shape file was rasterized and resampled to cell resolution of 30 × 30 m with a total of thirteen lithological units in the area as shown in Fig. 5.

Land use/land cover.

The Land use land cover (LULC) map was derived from Landsat-8 OLI/TRS images (courtesy of the United States Geological Survey (USGS) Earth Explorer) taken in October 2017 with cloud cover less than 10%. A supervised classification was performed using the Interactive supervised classification tool after selecting and merging training samples from the study area for each class. The five resulting classes are built-up area, agricultural land, barren land, forest (evergreen, deciduous), snow/glaciers and water bodies.

LULC map (Fig. 4h) can be associated to landslide occurrences since it illustrates the extent of human activity, agricultural land use, degree of deforestation amongst others.

Distance from faults/lineaments.

Landslides are more likely to occur in faulted and fractured regions which leads to inhomogeneity thereby reducing their stability and strength.

Buffer zones at interval of 200 m were created from the merged faults/lineaments shape file. The resulting map (Fig. 4f) was rasterized with 30 m cell resolution and reclassified into six categories namely 0–200 m, 200–400 m, 400–600 m, 600–800 m, 800–1000 m and >1000 m.

Distance to roads.

Road widening and construction in hilly areas often lead to vegetation removal, change in drainage pattern and alteration to slope profiles through slope-cutting process, all contributing to slope instability [12]. The road networks considered for analysis in the area consists of national highway, major district roads and local roads to better assess the spatial relationship between road network and landslide occurrence.

The resulting map was rasterized with 30 m cell resolution and reclassified into six categories with 200 m buffering intervals namely 0–200 m, 200–400 m, 400–600 m, 600–800 m, 800–1000 m and >1000 m.

5 Frequency Ratio Statistical Method

Frequency ratio, a data-driven statistical approach adopted in this study, has been used and validated by many researchers [1, 6, 8]. A table was created for all the nine landslide causative factors considered along with each of their classes.

The tabulate area tool was used to find out the pixel-wise contribution of every factor class to the training dataset of the updated landslide inventory for the calculation of frequency ratios (FR) as per Eq. (1).

$$\mathrm{FR} = \frac{P_L / \sum_{i=1}^{n} P_L}{P_C / \sum_{i=1}^{n} P_C} \tag{1}$$

where

P_L = Landslide pixels in a particular class.

$\sum_{i=1}^{n} P_L$ = Sum of all landslide pixels covering the area.

P_C = Pixels of a particular class.

$\sum_{i=1}^{n} P_C$ = Sum of all pixels covering the area.

Values above unity signify high correlation, whereas values less than unity demonstrate low correlation. The results are summarized in Table 1.

The FR values were then used for the reclassification of each of the nine causative thematic maps in the GIS platform for the final susceptibility map preparation using the Landslide Susceptibility Index (LSI) values [11] computed as per Eq. (2).

$$\mathrm{LSI} = \left(\mathrm{FR_{Slo}} + \mathrm{FR_{Asp}} + \mathrm{FR_{Curv}} + \mathrm{FR_{Lulc}} + \mathrm{FR_{Lith}} + \mathrm{FR_{Ele}} + \mathrm{FR}_{D_R} + \mathrm{FR}_{D_D} + \mathrm{FR}_{D_{F/L}}\right) \tag{2}$$

where

$\mathrm{FR_{Slo}}$, $\mathrm{FR_{Asp}}$,… = Sum of frequency ratios of each factor.

The final landslide susceptibility map was created using the Raster Calculator tool and reclassified into five categories using Natural Jenks break method namely very low, low, moderate, high and very high as in Fig. 6.

6 Results and Discussions

The Landslide Density Index (LDI) was computed as per Eq. (3) for each susceptibility class to evaluate the quality of produced landslide susceptibility map [13]. The increasing order of LDI (Table 2) imply that the frequency of landslide occurrence increases with increasing (very low to very high) susceptibility class.

$$\mathrm{LDI} = \frac{\%\ \text{landslide pixels in susceptibility class}}{\%\ \text{class pixels in susceptibility class}} \tag{3}$$

Receiver operator characteristics (ROC) method was then used to assess the fitness and prediction accuracy of the model through the Area Under Curve (AUC) of the success rate curve and the prediction rate curve [10, 11] using the sampled training (70%) and validation (30%) datasets, respectively.

The computed AUC of the success rate curve (Fig. 7) and the prediction rate curve (Fig. 8) were 0.873 and 0.803, respectively, as shown in Fig. 5. This indicates that the model had 87.3% training accuracy and 80.3% prediction accuracy.

The fitness and prediction accuracy of this frequency ratio-based model were considered reasonable.

The frequency ratios computed as in Table 1 gives an insight about the landslide distribution in each factor class.

Table 1 Frequency ratio results for the nine factors considered

Land use land cover	Class pixels	% Class pixels	Landslide pixels	% Landslide pixels	FR
Built up	146,846	0.14516	23,400	0.17687	1.21842
Forest	308,834	0.3053	9900	0.07483	0.24511
Water Body	4629	0.00458	900	0.0068	1.48662
Snow/Glaciers	123,809	0.12239	1800	0.01361	0.11116
Barren Land	203,861	0.20153	15,300	0.11565	0.57385
Agricultural Land/Grass	223,609	0.22105	81,000	0.61224	2.76974
Slope (°)	Class pixels	% Class pixels	Landslide pixels	% Landslide pixels	FR
0–14	137,223	0.12973	5400	0.04082	0.31462
15–24	261,701	0.24741	18,900	0.14286	0.57741
25–33	321,808	0.30424	44,100	0.33333	1.09564
34–45	241,211	0.22804	49,500	0.37415	1.64071
>45	95,810	0.09058	14,400	0.10884	1.20164
Aspect	Class pixels	% Class pixels	Landslide pixels	% Landslide pixels	FR
Flat	87	0.00008	0	0	0
North	64,632	0.06111	8100	0.06122	1.00184
Northeast	125,781	0.11893	17,100	0.12925	1.08678
East	132,831	0.1256	20,700	0.15646	1.24576
Southeast	121,512	0.11489	19,800	0.14966	1.30259
South	121,435	0.1153	29,700	0.22449	1.94696
Southwest	156,412	0.11482	14,400	0.10884	0.94794
West	156,412	0.14789	14,400	0.10884	0.73596
Northwest	146,739	0.13875	4500	0.03401	0.24515
North	66,228	0.06262	3600	0.02721	0.43453
Profile curvature	Class pixels	% Class pixels	Landslide pixels	% Landslide pixels	FR
Convex	113,351	0.10555	16,200	0.12245	1.16009
Flat	669,252	0.6232	72,900	0.55102	0.88418
Concave	291,289	0.27125	43,200	0.32653	1.20382
Distance to road (m)	Class pixels	% Class pixels	Landslide pixels	% Landslide pixels	FR
0–200	138,618	0.13702	67,500	0.5102	3.72347
200–400	87,959	0.08695	6300	0.04762	0.54768
400–600	71,444	0.07062	3600	0.02721	0.3853

(continued)

Table 1 (continued)

Distance to road (m)	Class pixels	% Class pixels	Landslide pixels	% Landslide pixels	FR
600–800	59,745	0.05906	5400	0.04082	0.69112
800–1000	54,078	0.05346	11,700	0.08844	1.65435
>1000	599,789	0.59289	37,800	0.28571	0.4819
Distance to faults/ lineaments (m)	Class pixels	% Class pixels	Landslide pixels	% Landslide pixels	FR
0–200	95,610	0.09451	8100	0.06122	0.64781
200–400	87,818	0.08681	12,600	0.09524	1.09711
400–600	82,262	0.08132	9900	0.07483	0.92024
600–800	72,002	0.07117	4500	0.03401	0.47789
800–1,000	68,400	0.06761	11,700	0.08844	1.30796
>1000	605,541	0.59858	85,500	0.64626	1.07966
Distance to drainage (m)	Class pixels	% Class pixels	Landslide pixels	% Landslide pixels	FR
0–100	82,554	0.0861	15,300	0.11565	1.41715
100–200	69,486	0.06869	18,900	0.14286	2.07983
200–300	74,861	0.074	7200	0.05442	0.73543
300–400	61,776	0.06107	8100	0.06122	1.0026
>400	722,956	0.71464	82,800	0.62585	0.87575
Elevation (m)	Class pixels	% Class pixels	Landslide pixels	% Landslide pixels	FR
1050–2000	264,717	0.2603	101,700	0.76871	0.83979
2000–3000	430,533	0.42335	28,800	0.21769	0.14622
3000–4000	281,431	0.27674	1800	0.01361	0.05916
4000–4900	40,277	0.03961	0	0	0
Lithology	Class pixels	% Class pixels	Landslide pixels	% Landslide pixels	FR
Schist and quartzite	159,066	0.15724	8100	0.06122	0.38938
Carbonaceous slate, phyllite, limestone, quartzite	74,580	0.07372	1800	0.01361	0.18455
Carbonaceous slate, phyllite, quartzite	13,122	0.01297	0	0	0
Diamictite, shale, slate, sandstone, limestone	4463	0.00441	0	0	0
Sillimanite—kyanie bearing schist, quartzite	204,013	0.20167	60,300	0.45578	2.26007
White-green quartzite, phyllite, basic flows	197,575	0.1953	18,900	0.14286	0.73146

(continued)

Table 1 (continued)

Lithology	Class pixels	% Class pixels	Landslide pixels	% Landslide pixels	FR
Streaky and banded gneiss	23,534	0.02326	3600	0.02721	1.16969
Phyllite, quartzite with basic flows	13,721	0.01356	0	0	0
Schist, gneiss, migmatite, quartzite, marble	116,964	0.11562	2700	0.02041	0.17651
Schist, phyllite, quartzite	57,587	0.05692	4500	0.03401	0.59752
Slate, phyllite, quartzarenite, limestone, metabasics	87,693	0.08668	28,800	0.21769	2.51125
Granitoid, gneiss, migmatite	5695	0.00563	0	0	0
Gravel, pebble, sand, silt and clay	53,620	0.053	3600	0.02721	0.51338

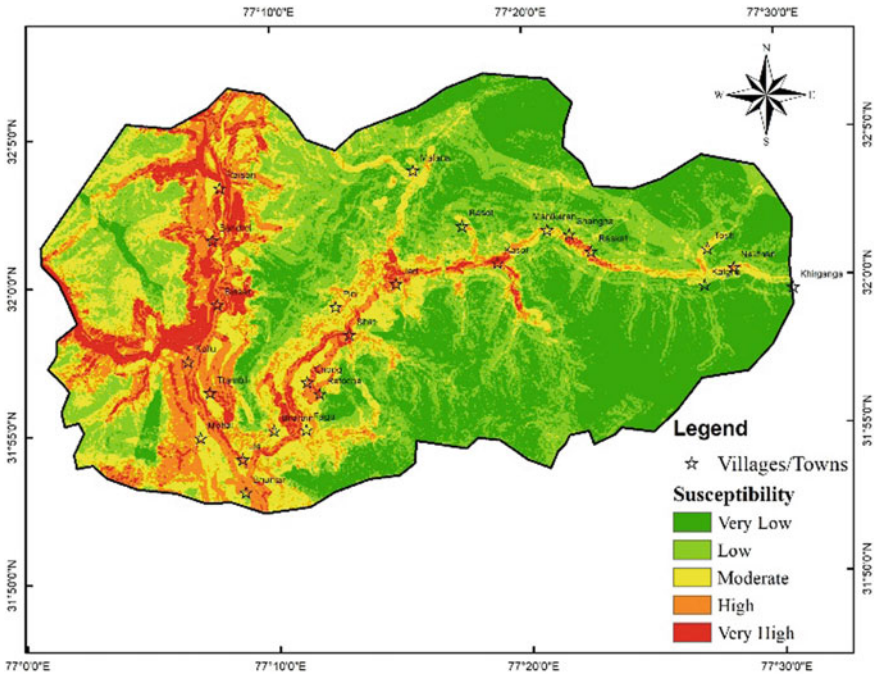

Fig. 6 Final landslide susceptibility map

Table 2 Landslide density index (LDI) calculation results

Susceptibility	Class pixels	% Class pixels	Landslide pixels	% Landslide pixels	LDI
Very low	335,136	0.33192	4500	0.07813	0.2354
Low	300,859	0.29797	9000	0.15625	0.5244
Moderate	183,862	0.18210	6300	0.10938	0.6006
High	136,632	0.13532	16,200	0.28125	2.0784
Very high	53,205	0.05269	21,600	0.37500	7.1166

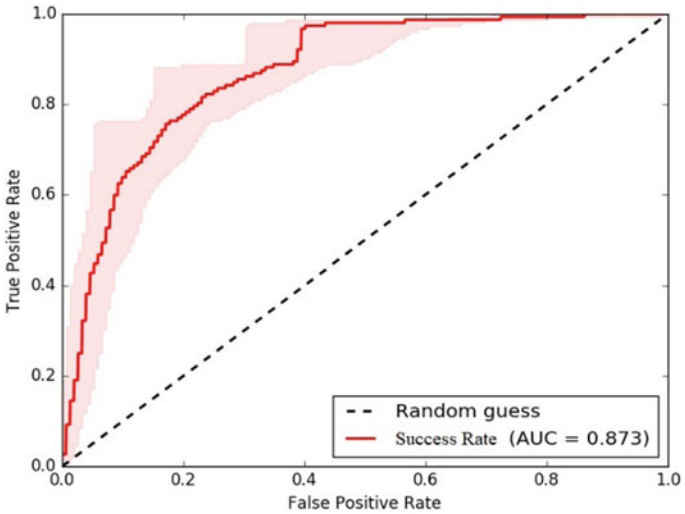

Fig. 7 Success rate curve

The LULC map showed highest landslide occurrences around the built-up area, agricultural land area and near water bodies, whilst the lowest being in the forest and snow/glaciers areas.

There was an increasing trend in landslide incidence as slope increased with highest value recorded for slope between 33° and 44°.

The south, south-east and east aspect were found more prone to landslides in the area whereas slope with no aspect had zero frequency ratio.

Convex and concave surfaces had highest values of frequency ratio compared to linear surfaces showing implication of convexity and concavity in landslide happening.

Increase in slope instability due to road construction in the area can be justified by the highest FR values (3.72347) obtained in the 0–100 m range of the buffered road network.

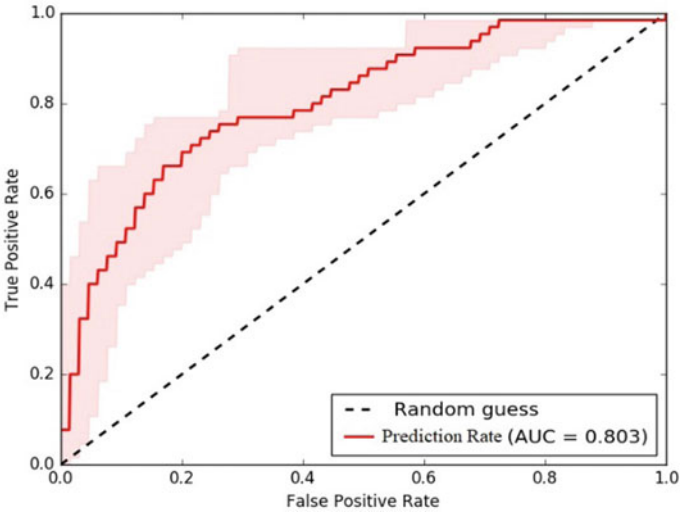

Fig. 8 Prediction rate curve

The highest frequency ratio values 1.41715 and 2.07983 for the drainage buffered zones of 0–100 m and 100–200 m, respectively, from the stream networks signify strong association to slope instability.

The lower two elevation zones (1050–2000 m and 2000–3000 m) have highest FR values (0.83979 and 0.14622) and also have more man-made activities compared to higher elevations in the area often covered with snow coupled with scarce human intervention and lesser extent of land.

For the lithologic contribution to landslides, the two groups namely slate, phyllite, quartzarenite, limestone, metabasics and sillimanite-kyanie bearing schist, quartzite have the highest FR values of 2.51125 and 2.26007, respectively, and out of thirteen, four groups had zero FR values, hence no contribution was observed.

7 Conclusion

The validation results showed reasonable prediction accuracy of the data-driven model adopted for mapping landslide susceptibility in this region using the nine selected factors. This model can be used for the generation of better landslide susceptibility maps for future planning and mitigation measures, but not as a replacement for detailed, localized studies performed by experts.

References

1. Avinash, K.G., Ashamanjari, K.G.: A GIS and frequency ratio-based landslide susceptibility mapping: Aghnashini river catchment, Uttara Kannada, India. Int. J. Geomat. Geosci. **1**(3), 343–354 (2010)
2. Bunn, M., Leshchinsky, B., Olsen, M., Booth, A.: A simplified, object-based framework for efficient landslide inventorying using LIDAR digital elevation model derivatives. Remote Sens. **11**(3)
3. Chandel, V.B.S., Brar, K.K., Chauhan, Y.: RS & GIS based landslide hazard zonation of mountainous terrains: a study from middle Himalayan Kullu District, Himachal Pradesh, India. Int. J. Geomat. Geosci. **2**(1), 121–132 (2011)
4. Chung, C.J.F., Fabbri, A.G.: Probabilistic prediction models for landslide hazard mapping. Photogramm. Eng. Remote. Sens. **65**(12), 1389–1399 (1999)
5. Dikau, R.: The recognition of landslides. In: Casale, R., Margottini, C. (Eds.) Floods and Landslides: Integrated Risk Assessment; Environmental Science. Springer, Science and Business Media: Berlin/Heidelberg, Germany (1999)
6. Fayez, L., Pazhman, D., Pham, B.T., Dholakia, M.B., Solanki, H.A., Khalid, M., Prakash, I.: Application of frequency ratio model for the development of landslide susceptibility mapping at part of Uttarakhand State, India. Int. J. Appl. Eng. Res. **13**(9), 6846–6854 (2018)
7. Kumar, A., Sharma, R., Bansal, V.: GIS-based landslide hazard mapping along NH-3 in mountainous terrain of Himachal Pradesh, India Using Weighted Overlay Analysis: IC_SWMD 2018 (2019)
8. Lee, S., Pradhan, B.: Landslide hazard mapping at Selangor, Malaysia using frequency ratio and logistic regression models. Landslides **4**(1), 33–41 (2007)
9. Mandal, S., Maiti, R.: Application of analytical hierarchy process (AHP) and frequency ratio (FR) model in assessing landslide susceptibility and risk. In: Semi-quantitative Approaches for Landslide Assessment and Prediction. Springer Natural Hazards. Springer, Singapore (2015)
10. Nohani, E., Moharrami, M., Sharafi, S., Khosravi, K., Pradhan, B., Pham, B.T., Lee, S., Melesse, A.M.: Landslide susceptibility mapping using different GIS-based bivariate models. Water **11**(7) (2019)
11. Pradhan, B.: Landslide susceptibility mapping of a catchment area using frequency ratio, fuzzy logic and multivariate logistic regression approaches. J. Indian Soc. Remote Sens. **38** (2), 301–320 (2010)
12. Ramani, S., Rajamanickam, G.V., Pichaimani, K.: Landslide susceptibility analysis using Probabilistic Certainty Factor Approach: a case study on Tevankarai stream watershed, India. J. Earth Syst. Sci. **121**(5)
13. Sarkar, S., Kanungo, D.P.: An integrated approach for landslide susceptibility mapping using remote sensing and GIS. Photogramm. Eng. Remote. Sens. **70**, 617–625 (2004)